

Rotating Dirac fermions in a magnetic field in 1+2,3 dimensions

Yizhuang Liu and Ismail Zahed*

Department of Physics and Astronomy, Stony Brook University, Stony Brook, New York 11794-3800, USA

(Dated: December 14, 2024)

We consider the effects of an external magnetic field on rotating fermions in 1+2,3 dimensions. The dual effect of a rotation parallel to the magnetic field causes a net increase in the fermionic density by centrifugation, which follows from the sinking of the particle lowest Landau level in the Dirac sea for free Dirac fermions. In $1+d = 2n$ dimensions, this effect is related to the chiral magnetic effect in $2n-2$ dimensions. This phenomenon is discussed specifically for both weak and strong inter-fermion interactions in 1+2 dimensions. For QCD in 1+3 dimensions with Dirac quarks, we show that in the strongly coupled phase with spontaneously broken chiral symmetry, this mechanism reveals itself in the form of an induced pion condensation by centrifugation. We use this observation to show that this effect causes a shift in the chiral condensate in leading order in the pion interaction, and to discuss the possibility for the formation of a novel pion super-fluid phase in present heavy ion collisions at collider energies.

PACS numbers:

I. INTRODUCTION

The combined effects of rotations and magnetic fields on Dirac fermions are realized in a wide range of physical settings ranging from macroscopic spinning neutron stars and black holes [1], all the way to microscopic anomalous transport in Weyl metals [2]. In any dimensions, strong magnetic fields reorganize the fermionic spectra into Landau levels, each with a huge planar degeneracy that is lifted when a parallel rotation is applied. The past decade has seen a large interest in the chiral and vortical effects and their relationship with anomalies [3] (and references therein).

Perhaps, a less well known effect stems from the dual combination of a rotation and magnetic field on free or interacting Dirac fermions. Recently, it was noted that this dual combination could lead to novel effects for composite fermions at half filling in 1+2 dimensions under the assumption that they are Dirac fermions [4], and more explicitly for free and interacting Dirac fermions in 1+3 dimensions [5–7]. Indeed, when a rotation is applied along a magnetic field, the charge density was observed to increase *in the absence* of a chemical potential. A possible relationship of this phenomenon to the Chern-Simons term in odd dimensions, and the chiral anomaly in even dimensions was suggested.

The purpose of this paper is to revisit these issues in a more explicit way in 1+2,3 dimensions. The case of 1+2 dimensions is of interest to planar materials in the context of solid state physics, while the case of 1+3 dimensions is of more general interest with relation to QCD. Recently, there have been few studies along these lines using effective models of the NJL type in 1+3 dimensions, where the phenomenon of charge density enhancement

was also confirmed with new observations [6, 7].

This paper consists of a number of new results: 1/ a full analysis of the combined effects of a rotation and magnetic field on free and interacting Dirac fermions in 1+2 dimensions, both at weak and strong coupling; 2/ a correspondence with anomalies in arbitrary dimensions; 3/ a deformation of the current densities by centrifugation in the presence of a magnetic field; 4/ a depletion of the QCD chiral condensate in leading order in the pion interaction; 5/ a charge pion condensation induced by centrifugation in a magnetic field.

The outline of the paper is as follows: In section II we detail the Landau level problem for free Dirac fermions in 1+2 dimensions in the presence of an arbitrary rotation described using a local metric. In section III we explore the effects of the interaction on the free results through a 4-Fermi interaction both in the weak and strong coupling regime. In section IV we extend our chief observations to 1+3 dimensions with particular interest to the shift in the chiral condensate in QCD, and the formation of a pion super-fluid phase in heavy ion collisions. Our conclusions are in section V. We record in the Appendices useful details regarding some of the calculations.

II. DIRAC FERMIONS IN 1+2

In this section we will outline how to implement a global rotation through a pertinent metric. We will then use it to derive explicit results for massless Dirac fermions with a global $U(2)$ symmetry in the presence of a parallel magnetic field in 1+2 dimensions. The basic mechanism of the shift caused by the rotation on the LLL will be clearly elucidated, and both the scalar and vector densities evaluated.

*Electronic address: yizhuang.liu@stonybrook.edu; Electronic address: ismail.zahed@stonybrook.edu

A. Metric for a rotating frame

To address the effects of a finite rotation Ω in 1 + 2 dimensions we define the rotating metric

$$ds^2 = (1 - \Omega^2 \rho^2) dt^2 + 2y\Omega dx dt - 2x\Omega dy dt \quad (1)$$

The frame fields or veilbeins are defined as $g^{\mu\nu} = e_a^\mu e_b^\nu \eta_{ab}$ with signature $\sqrt{-g} = 1$, in terms of which the co-moving frame is $\theta^a = e_a^\mu dx^\mu$ and $e_a = e_a^\mu \partial_\mu$ are explicitly given by

$$\begin{aligned} (\theta^0, \theta^1, \theta^2) &= (dt, dx - y\Omega dt, dy + x\Omega dt) \\ (e_0, e_1, e_2) &= (\partial_t + y\Omega \partial_x - x\Omega \partial_y, \partial_1, \partial_2) \end{aligned} \quad (2)$$

with the spin connections

$$\begin{aligned} \omega_0^1 &= \omega_1^0 = +\Omega(dy - \Omega x dt) \\ \omega_0^2 &= \omega_2^0 = -\Omega(dx + \Omega y dt) \end{aligned} \quad (3)$$

In a fixed area of size $S = \pi R^2$, the time-like nature of the metric (1) and therefore causality are maintained for $\Omega R \leq 1$. The importance of a finite size for rotating fermions was emphasized in [7]. This will be understood throughout.

B. Rotation plus magnetic field

The Lagrangian that describes free rotating Dirac fermions in a fixed magnetic field in 1 + 2 dimensions, reads

$$\begin{aligned} \mathcal{L} &= \bar{\psi}(i\gamma^\mu(D_\mu + \Gamma_\mu) - M)\psi \\ &= \bar{\psi}(i\gamma^0(\partial_t - \Omega(x\partial_y - y\partial_x + iS^z)) + i\gamma^i D_i - M)\psi \end{aligned} \quad (4)$$

with the long derivative $D = \partial - ieA$, and the following choice of gamma matrices, γ^a as $\gamma^0 = \text{diag}(\sigma_3, -\sigma_3), \gamma^1 = \text{diag}(i\sigma_1, -i\sigma_1), \gamma^2 = \text{diag}(i\sigma_2, -i\sigma_2)$, to accommodate for both particles and anti-particles.

A thorough analysis of (4) for an external vector potential in a rotationally non-symmetric gauge was given in [11]. Here we insist on preserving rotational symmetry by choosing $A_\mu = (0, By/2, -Bx/2, 0)$. As a result, the LL spectrum is characterized explicitly by both energy and angular momentum conservation which are described in terms of the anti-commutative harmonic oscillator a, b operators

$$\begin{aligned} a &= \frac{i}{\sqrt{2eB}}(D_x + iD_y) = -\frac{i}{\sqrt{2eB}}\left(2\bar{\partial} + \frac{eBz}{2}\right) \\ b &= \frac{1}{\sqrt{2eB}}\left(2\partial + \frac{eB\bar{z}}{2}\right) \end{aligned} \quad (5)$$

Throughout, we will assume $eB > 0$ unless specified otherwise. The rotating Landau levels are labelled by m, n as

$$E^\pm + \Omega(m - n + \frac{1}{2}) = \pm\sqrt{M^2 + 2eBn} = \pm\tilde{E} \quad (6)$$

for particles and anti-particles. The corresponding normalized scalar wave functions for the n -th Landau level with good angular momentum $l_z = xp_y - yp_x = b^\dagger b - a^\dagger a$ with eigenvalue $m - n$, are

$$f_{nm} = \frac{(a^\dagger)^n (b^\dagger)^m}{\sqrt{n!m!}} f_{00} \quad (7)$$

with the lowest Landau level (LLL) $f_{00} \propto e^{-\frac{1}{4}eB(x^2+y^2)}$. Note that for $n=0$, we have only one positive energy state with spin up, and one negative energy state with spin down, each with degeneracy $N = eBS/2\pi$. For $\Omega = 0$ and $n > 0$ all Landau level (LL) have degeneracy $2N = eBS/\pi$. The degeneracy is lifted by centrifugation for $\Omega \neq 0$.

In terms of (7) the quantized Dirac fields follow in the form

$$\psi(t, \vec{x}) = \sum_{nmi} (u_{nm}^i(\vec{x}) e^{-iE^+ t} a_{nm}^i + v_{nm}^i(\vec{x}) e^{-iE^- t} b_{nm}^{\dagger i}) \quad (8)$$

where a_{nm}^i annihilates a particle with positive energy E^+ and spin $i = \pm\frac{1}{2}$, and $b_{nm}^{\dagger i}$ creates a hole with negative energy E^- and spin $i = \mp\frac{1}{2}$. Their corresponding wave-functions are

$$\begin{aligned} u_{0m} &= (f_{0m}, 0, 0, 0) \\ v_{0m} &= (0, 0, f_{0m}, 0) \\ u_{nm}^+ &= \sqrt{\frac{\tilde{E} + M}{2\tilde{E}}} \left(f_{nm}, \frac{i\sqrt{2eB}}{\tilde{E} + M} f_{n-1,m}, 0, 0 \right) \\ u_{nm}^- &= \sqrt{\frac{\tilde{E} - M}{2\tilde{E}}} \left(0, 0, f_{nm}, -\frac{i\sqrt{2eB}}{\tilde{E} - M} f_{n-1,m} \right) \\ v_{nm}^+ &= \sqrt{\frac{\tilde{E} - M}{2\tilde{E}}} \left(f_{nm}, -\frac{i\sqrt{2eB}}{\tilde{E} - M} f_{n-1,m}, 0, 0 \right) \\ v_{nm}^- &= \sqrt{\frac{\tilde{E} + M}{2\tilde{E}}} \left(0, 0, f_{nm}, \frac{i\sqrt{2eB}}{\tilde{E} + M} f_{n-1,m} \right) \end{aligned} \quad (9)$$

C. Scalar density

For $M = 0$, (4) exhibits a $U(2)$ symmetry as the set $(\mathbf{1}, \gamma^5, -i\gamma^3, \gamma^{1+2} = -i\gamma^0\gamma^1\gamma^2)$ leaves (4) unchanged. This symmetry rotates particles to anti-particles. The

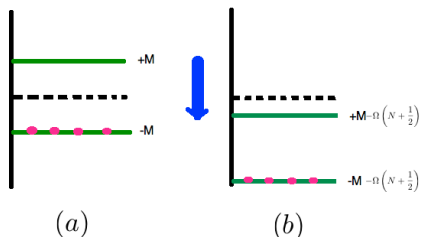


FIG. 1: The particle (+ M) and anti-particle ($-M$) LLL for $\Omega = 0$ are shown in (a) each with degeneracy N . For $\Omega \neq 0$ the degeneracy is lifted. In (b) we illustrate how the centrifugation lifts the degeneracy on the states with angular momentum N by shifting them down by $\pm M - \Omega(N + \frac{1}{2})$. The rotating vacuum now includes the particle LLL which needs to be filled.

mass upsets this symmetry, and is only $U(1) \times U(1)$ symmetric under the action of $(\mathbf{1}, \gamma^{1+2})$. In [11] it was noted, that for $\Omega = 0$, (4) breaks spontaneously $U(2) \rightarrow U(1) \times U(1)$ with a finite condensate $\langle \bar{\psi}\psi \rangle = -N/S$ without fermionic interactions. This is readily understood from the illustration in Fig. 1a, where only the LLL for particle states with spin up and mass $+M$, and antiparticle states with spin down and mass $-M$ are shown. Each level is N degenerate. The vacuum state consists of filling the anti-particle states only. Clearly, for finite M the $U(2)$ symmetry is explicitly broken. However, as $M \rightarrow 0$ the explicit breaking is removed, but the anti-particle states remain still occupied even though they have the same zero energy as the particle states. The state breaks spontaneously the balance between particles and anti-particles or $U(2) \rightarrow U(1) \times U(1)$. We now show that this *free* scalar condensate disappears for any finite rotation Ω .

For a heuristic arguments for the role of a finite rotation Ω along the magnetic field, we show in Fig. 1b its effect on the LLL with maximum orbital angular momentum N . Both the particle and anti-particle states are shifted down and below the zero energy mark even for $M = 0$. This means that in the rotating vacuum, the particle LLL needs to be filled. Since typically the unordered scalar condensate operator is $\bar{\psi}\psi \sim (a^\dagger a + b^\dagger b - 1)\bar{u}u$, it follows for Fig. 1b that $\bar{\psi}\psi \sim (1 + 0 - 1)\bar{u}u = 0$.

Formally, the scalar condensate carried by the rotating LLL can be explicitly constructed using the fermionic field operator (8). At finite temperature $1/\beta$ and Ω , it is readily found in the form

$$\begin{aligned} \langle \bar{\psi}\psi \rangle(r) &= \frac{eB}{2\pi} \sum \frac{e^{-\frac{eBr^2}{2}}}{m!} \left(\frac{eBr^2}{2} \right)^m \\ &\times (n_F(-\beta\Omega(m + 1/2)) + n_F(\beta\Omega(m + 1/2)) - 1) = 0 \end{aligned} \quad (10)$$

which is identically zero even for zero temperature $\beta = \infty$. So any finite rotation, however infinitesimal will cause the scalar density to vanish for free rotating fermions at finite B in 1 + 2 dimensions.

D. Vector density

The local density of Dirac fermions in the rotating frame in 1 + 2 dimensions is readily found using (8) in the current density

$$\langle j^0(x) \rangle = \langle : \bar{\psi}\gamma^0\psi : \rangle = \sum_{n=0} j_n^0(x) \quad (11)$$

The normal ordering is carried with respect to the true vacuum at finite Ω . Each LL in (11) including the LLL contribute through a tower of rotational states $-n < m < N - n$ for both particles and anti-particles. This finite range in the angular momentum is further detailed in Appendix I. Specifically, and for finite temperature $1/\beta$, the contributions of the LL and the LLL are respectively

$$\begin{aligned} j_{n>0}^0(x) &= \sum_m |f_{nm}|^2 + |f_{n-1,m}|^2 \\ &\times (n_F(E_{nm}^+) - n_F(E_{nm}^-)) \\ j_{n=0}^0(x) &= \frac{eB}{2\pi} \sum_m \frac{e^{-\frac{eBr^2}{2}}}{m!} \left(\frac{eBr^2}{2} \right)^m \\ &\times \frac{\sinh(\beta\Omega(m + \frac{1}{2})/2)}{\cosh(\beta\Omega(m + \frac{1}{2})/2)} \end{aligned} \quad (12)$$

with the definition

$$\begin{aligned} E_{nm}^\pm &= E_n \mp \left(m - n + \frac{1}{2} \right) \Omega \\ &= \sqrt{eBn} \mp \left(m - n + \frac{1}{2} \right) \Omega \end{aligned} \quad (13)$$

We first note that the particle density is inhomogeneous in the plane and peaks at the edge of the disc $S = \pi R^2$ under the effects of centrifugation. For small $\beta\Omega \ll 1$, i.e. small rotations or high temperature, the inhomogeneous particle density carried by the LLL is

$$\begin{aligned} j_0^0|_\Omega(r) &= \beta\Omega \frac{eB}{4\pi} \sum_m \frac{e^{-\frac{eBr^2}{2}}}{m!} \left(\frac{eBr^2}{2} \right)^m \left(m + \frac{1}{2} \right) \\ &= \frac{\beta\Omega eB}{4\pi} \frac{1 + eBr^2}{2} \end{aligned} \quad (14)$$

Under the combined effect of the rotation and the magnetic field the particle density undergoes a *centrifuge effect* with a maximum at the edge of the rotational plane. This effect will persist even in the presence of interactions as we will discuss below (see Fig. 6).

The total number of particles follow from (11-13) by integration over $S = \pi R^2$. The results for the LL and LLL are respectively

$$\begin{aligned} n_n &= 2 \sum_m (n_F(E_{nm}^+) - n_F(E_{nm}^-)) \\ n_0 &= \sum_m \frac{\sinh(\beta\Omega(m + \frac{1}{2})/2)}{\cosh(\beta\Omega(m + \frac{1}{2})/2)} \end{aligned} \quad (15)$$

For small $\beta\Omega$, which is similar to small Ω or large temperature, the results in (15) simplify

$$\begin{aligned} n_n|_{\Omega} &= 4\beta\Omega \sum_m \left(m - n + \frac{1}{2}\right) \frac{e^{\beta E_n}}{(1 + e^{\beta E_n})^2} \\ &= 4\beta\Omega \left(\frac{N^2 + 2N}{2} - n\right) \frac{e^{\beta E_n}}{(1 + e^{\beta E_n})^2} \\ n_0|_{\Omega} &= \frac{1}{2}\beta\Omega \sum_m \left(m + \frac{1}{2}\right) = \frac{\beta\Omega(N^2 + 2N)}{4} \end{aligned} \quad (16)$$

We note that in 1 + 2 dimensions, the LLL generates a net density at $\beta\Omega \ll 1$. For strictly zero temperature (15) gives the exact result

$$n_0|_{\beta=\infty} = \text{sgn}(\Omega)N \quad (17)$$

which can be understood from Fig. 1b for $M \rightarrow 0$. Since the *normal ordered* density operator : $\psi^\dagger\psi$: $\sim (a^\dagger a - b^\dagger b)u^\dagger u \sim (1 - 0)u^\dagger u$ which precisely gives N . Note that for a rotation opposite to the magnetic field, the LLL shift up and above the zero energy mark. Therefore, we have instead : $\psi^\dagger\psi$: $\sim (a^\dagger a - b^\dagger b)u^\dagger u \sim (0 - 1)u^\dagger u$ which precisely gives $-N$, as expected from (17).

These observations are not restricted to only finite temperature. Indeed, at zero temperature but finite chemical potential, the rotation induces changes in the population of the LLL. This can be seen through the substitution [7, 8]

$$\beta\Omega \left(m + \frac{1}{2}\right) \rightarrow \beta \left(\mu + \Omega \left(m + \frac{1}{2}\right)\right) \quad (18)$$

in (15), with the result

$$\begin{aligned} n_0(\mu) &= N, & \mu &\geq -\frac{\Omega}{2} \\ n_0(\mu) &\approx N + 1 + \frac{2\mu}{\Omega}, & -\left(N + \frac{1}{2}\right)\Omega &\leq \mu \leq -\frac{\Omega}{2} \\ n_0(\mu) &= -N, & \mu &\leq -\left(N + \frac{1}{2}\right)\Omega \end{aligned} \quad (19)$$

III. INTERACTING FERMIONS IN 1 + 2

Consider now fermions in 1 + 2 dimensions interacting via 4-Fermi interactions, as a way to model QCD₁₊₂ in strong and rotating magnetic fields. The advantage of this reduction is that it will allow for closed form results with physical lessons for QCD₁₊₃ dimensions, which even when modeled with 4-Fermi interactions is only tractable numerically. Following [11, 12], we now consider N_c copies of the preceding Dirac fermions, interacting via local 4-Fermi $U(2)$ symmetric interactions

$$\mathcal{L}_{\text{int}} = \frac{G}{2} (|\bar{\psi}\psi|^2 + |\bar{\psi}i\gamma^5\psi|^2 + |\bar{\psi}\gamma^3\psi|^2) \quad (20)$$

Standard bosonization gives

$$\mathcal{L}_{\text{int}} \rightarrow -\bar{\psi}(\sigma + \gamma^3\tau + i\gamma^5\pi)\psi - \frac{1}{2G}(\sigma^2 + \pi^2 + \tau^2) \quad (21)$$

with the scalar fields

$$-\frac{1}{G}(\sigma, \tau, \pi) = (\bar{\psi}\psi, \bar{\psi}\gamma^3\psi, i\bar{\psi}\gamma^5\psi) \quad (22)$$

For large N_c , (92) can be analyzed in the leading $1/N_c$ approximation using the loop expansion for the effective action. Explicit $U(2)$ symmetry makes the effective action only a function of $\sigma^2 + \tau^2 + \pi^2$, so it is sufficient to search for saddle points with $\tau = \pi = 0$, as others follow by symmetry.

The effective potential stemming from (92) can be organized in three parts

$$\mathcal{V} = \mathcal{V}_0 + \mathcal{V}_T = \frac{\sigma^2}{2G} + \mathcal{V}_\Lambda + \mathcal{V}_T \quad (23)$$

The zero temperature (vacuum) contribution from the fermion loop is

$$\mathcal{V}_\Lambda = -\frac{N_c}{4\pi^{\frac{3}{2}}} \int_{\frac{1}{\Lambda^2}}^{\infty} \frac{ds}{s^{\frac{3}{2}}} e^{-s\sigma^2} eB \coth(eBs) \quad (24)$$

which is cut off in the UV by $1/\Lambda^2$, while the thermal contribution is

$$\mathcal{V}_T = -\frac{N_c T}{S} \sum_{j=1, -1} \sum_{n=0}^N \sum_{l=-n}^{N-n} \ln(1 + e^{-\beta(E_n - j\Omega(l + \frac{1}{2}))}) \quad (25)$$

with $E_n = \sqrt{\sigma^2 + 2eBn}$ and $N/S = eB/2\pi$. A complementary but numerically useful approximation to (25) is given in Appendix II using the proper time formalism.

A. Weak coupling regime

At zero temperature and in the absence of B, Ω , the effective potential (94) for the interacting Dirac fermions in $1 + 2$ dimensions simplifies

$$\mathcal{V} \rightarrow \frac{\sigma^2}{2G} - \frac{N_c}{4\pi^{\frac{3}{2}}} \int_{\frac{1}{\Lambda^2}}^{\infty} \frac{ds}{s^{\frac{5}{2}}} e^{-s\sigma^2} \quad (26)$$

If we set $g = \frac{G\Lambda}{\pi}$, then (26) exhibits a minimum at $\sigma = \Lambda/g_r$ with $1/g_r = 1/g - 1/g_c$, only for sufficiently strong coupling $g > g_c = \sqrt{\pi}$. The minimum breaks spontaneously $U(2) \rightarrow U(1) \times U(1)$ with a finite $\langle \bar{\psi}\psi \rangle = -N_c\sigma/G$. The putative chargeless Goldstone mode signals a BKT phase at any finite N_c .

At zero temperature and zero rotation $\Omega = 0$ but with $B \neq 0$, the effective potential (94) can be made more explicit by rescaling and expanding in $1/\Lambda$. For small σ and large Λ the dominant contributions are

$$\begin{aligned} \mathcal{V}_\Lambda = & + \frac{N_c\Lambda^3}{4\pi^{\frac{3}{2}}} \int_1^\infty \frac{dx}{s^{\frac{3}{2}}} \frac{eBx}{\Lambda} \coth\left(\frac{eBx}{\Lambda}\right) \\ & - \frac{N_c\Lambda\sigma^2}{2\pi^{\frac{3}{2}}} + \frac{N_c\sigma^3}{3\pi} \\ & + \frac{N_c}{4\pi^{\frac{3}{2}}} \int \frac{ds}{s^{\frac{5}{2}}} (e^{-s\sigma^2} - 1)(eBs \coth(eBs) - 1) \\ & + \mathcal{O}\left(\frac{1}{\Lambda}\right) \end{aligned} \quad (27)$$

The first contribution is independent of σ , so we will ignore it. Therefore, the vacuum contribution to the effective potential combines the first term in (94) and the second and third contributions in (27)

$$\frac{\mathcal{V}_0}{N_c} \approx \frac{\Lambda\sigma^2}{2\pi g_r} - \frac{eB}{2\pi}\sigma + \frac{\sigma^3}{3\pi} \quad (28)$$

In the weak coupling regime

$$0 \leq \left(\frac{1}{g_r} \equiv \frac{1}{g} - \frac{1}{g_c}\right)^{-1} \leq \frac{\Lambda}{eB} \quad (29)$$

we can ignore the cubic contribution in (28). A minimum of (28) always exists for arbitrarily weak coupling, with a mass gap $\sigma = \pi g_r N/S\Lambda$ and a finite chiral condensate $\langle \bar{\psi}\psi \rangle = -N_c N/S(1 - g/g_c) \approx -N_c N/S$. The latter is in agreement with the result for free Dirac fermions. This is the phenomenon of magnetic catalysis [11].

1. Vacuum with $\Omega \neq 0$

At zero temperature, the effective potential for rotating Dirac particles in a strong magnetic field is given by

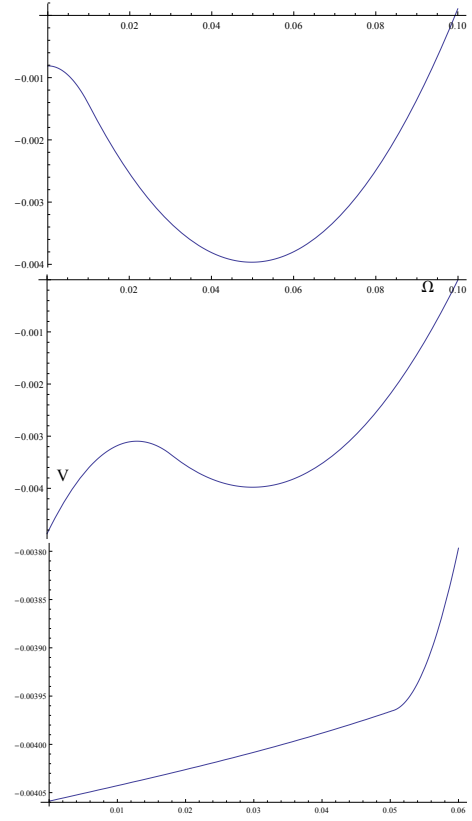


FIG. 2: Effective potential \mathcal{V} as a function of σ in units of \sqrt{eB} at $T = 0$: $\Omega = 0.0001\sqrt{eB}$ (top); $\Omega = 0.00049\sqrt{eB}$ (middle); $\Omega = 0.0005\sqrt{eB}$ (bottom).

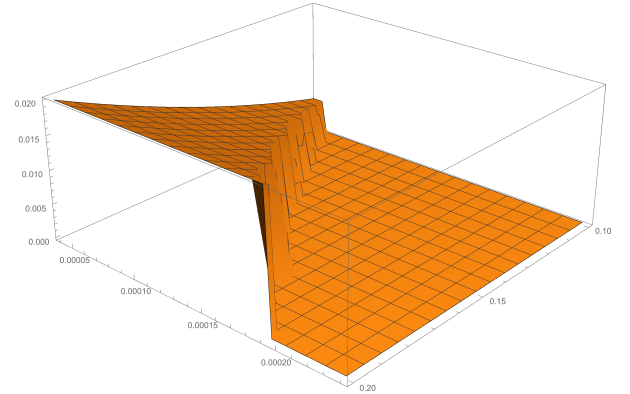


FIG. 3: Effective mass as a function of \sqrt{eB} and Ω in units of Λ . The mass gap disappears for $\Omega \geq \Omega_c$ as given by (35) through a first order transition.

the first two contributions in (94) plus the contribution from the rotating anti-particles in the LL,

$$\begin{aligned} \frac{\mathcal{V}}{N_c} = & + \frac{\Lambda\sigma^2}{2\pi g_r} - \frac{eB}{2\pi}\sigma \\ & - \frac{eB}{2\pi N} \sum_{l=0}^N \left(\left(l + \frac{1}{2} \right) \Omega - \sigma \right) \theta \left(\left(l + \frac{1}{2} \right) \Omega - \sigma \right) \end{aligned} \quad (30)$$

For small rotation the summation can be approximated by a continuous integration with the result

$$\frac{\mathcal{V}}{N_c} \approx \frac{\Lambda\sigma^2}{2\pi g_r} - \frac{eB}{2\pi}\sigma - \frac{1}{2\Omega S} \theta(E_\Omega - \sigma)(E_\Omega - \sigma)^2 \quad (31)$$

with $E_\Omega = (N + \frac{1}{2})\Omega$. For $\sigma > E_\Omega$, the effective potential is independent of Ω , and develops a minimum for

$$\begin{aligned} \sigma_2 = & + \frac{\pi g_r}{\Lambda} \frac{eB}{2\pi} \\ \frac{\mathcal{V}_2}{N_c} = & - \frac{\pi g_r}{2\Lambda} \left(\frac{eB}{2\pi} \right)^2 \end{aligned} \quad (32)$$

In contrast, for $\sigma < E_\Omega$, (31) depends on Ω through

$$\frac{\mathcal{V}}{N_c} \approx \left(\frac{\Lambda}{2\pi g_r} - \frac{eB}{4\pi N\Omega} \right) \sigma^2 + \frac{eB}{4\pi N} \sigma - \frac{eB\Omega}{4\pi} \left(N + \frac{1}{2} \right) \quad (33)$$

and prefers always

$$\begin{aligned} \sigma_1 = & 0 \\ \frac{\mathcal{V}_1}{N_c} = & - \frac{E_\Omega}{2} \frac{eB}{2\pi} \end{aligned} \quad (34)$$

For $E_\Omega < \frac{\pi g_r}{\Lambda} \frac{eB}{2\pi}$ the 2-minimum (34) is dominant. The rotating vacuum develops a scalar condensate $\langle \bar{\psi}\psi \rangle \neq 0$ with finite σ_2 but zero fermion density $\langle \bar{\psi}\gamma^0\psi \rangle = 0$. In the opposite, with $E_\Omega > \frac{\pi g_r}{\Lambda} \frac{eB}{2\pi}$, the 1-minimum (34) takes over. The rotating vacuum prefers a gapless solution with $\sigma_1 = 0$ and zero scalar condensate $\langle \bar{\psi}\psi \rangle = 0$, but a finite fermion density $\langle \bar{\psi}\gamma^0\psi \rangle \neq 0$. In large N , the critical value for which this occurs is

$$\Omega_c = \frac{g_r}{2N+1} \frac{eB}{\Lambda} \quad (35)$$

This is the phenomenon of rotational inhibition of the magnetic catalysis noted in 1 + 3 dimensions in [7]. At finite but large N and without the use of the continuum approximation and keeping the σ^3 term, the results remain quantitatively almost the same, with one exception that the local minimum $\sigma_1 = 0$ can overtake the finite local minimum σ_2 slightly before the Ω_c . For $\Lambda = 10\sqrt{eB}$ and $N = 100$, (35) yields $\Omega_c = 0.000497\sqrt{eB}$. We note

that in the free case with $\Lambda \rightarrow \infty$, (35) yields $\Omega_c \rightarrow 0$ in agreement with the observation in (10). Any finite rotation destroys the free scalar condensate.

In Fig. 2 we show the behavior of the effective potential for finite but small Ω with the two local minima (32) and (34). We have used $\Lambda/\sqrt{eB} = 10$, $N = 100$ and $g_r = 1$. A transition sets in numerically $\Omega_c = 0.000488\sqrt{eB}$ in agreement with (35). In Fig. 3 we display the effective mass as a function of \sqrt{eB} and Ω in units of Λ , for $g_r = 1$ (weak coupling regime) and $T = 0$. While the mass gap is seen to increase slightly faster than linearly with \sqrt{eB} at $\Omega = 0$, the effects of the rotation is to cause it to disappear at the critical value (35) through a first order transition at weak coupling.

2. Thermal state with $\Omega \neq 0$

First we note that the existence of a mass gap for any finite temperature does not contradict the Mermin-Wagner-Coleman (MWC) theorem, since the thermal state is in a BKT phase rather than a spontaneously broken or Goldstone phase. Having said that, at finite temperature and weak coupling, we note that since $\sigma_2 \ll \sqrt{eB}$, the temperatures of interest for the vanishing of the mass gap, are in the low range with $T \ll \sqrt{eB}$. Therefore, only the $j = \pm 1$ LLL contribute in (25). For $T \approx T_c \approx \sigma_2$, the potential flattens out and the centrifugation near $\sigma = 0$ becomes visible leading to a small value for the critical Ω_c .

In Fig. 4 we show the behaviour of the effective potential for $\Lambda/\sqrt{eB} = 10$, $N = 100$ and $g_r = 1$ (weak coupling) for $\beta = 80/\sqrt{eB}$ and $\beta = 43/\sqrt{eB}$. For $\beta \geq 80/\sqrt{eB}$ the transition occurs at $\Omega_c \approx 0.0005\sqrt{eB}$, and for $\beta = 43/\sqrt{eB}$, the transition is around $\Omega_c = 0.0001\sqrt{eB}$. The critical temperature is numerically in the range $\beta_c \approx (40-43)/\sqrt{eB}$. The behavior of the effective mass is shown in in Fig. 5 for the same value of $g_r = 1$ (weak coupling) and $\Lambda = 10\sqrt{eB}$, as a function of β and Ω for the ranges $50 < \beta < 80$ and $0.0003 \leq \Omega \leq 0.0006$ in units of \sqrt{eB} .

In Fig. 6 we show the analogue of the profile density (14) in units of \sqrt{eB} , in the weak coupling regime with $g_r = 1$ and for $1/\beta \ll \Omega$ as a function of $x = eBr^2/2$. The first figure from the top is for $\Omega = 0.00005\sqrt{eB}$ for $1/\beta = 0$. It is roughly constant and drops sharply at the edge of the causality disc fixed by $\Omega R = 1$. However, for $\Omega \ll 1/\beta \ll \sqrt{eB}$ a linear behavior sets in the middle of the disc, to drop only sharply at the edge. The second and third figures from the top are for $\beta = 100/\sqrt{eB}$ and $\Omega = 0.0001\sqrt{eB}$ and $\Omega = 0.0005\sqrt{eB}$ respectively. The fourth figure is for $\beta = 40/\sqrt{eB}$ at $\Omega = 0.0001\sqrt{eB}$. As we indicated in section IID for the free case, this *centrifugation effect* holds for the interacting case as well and carries to higher dimensions as we show below. We will suggest a possible physical application in 1+3 dimensions. Finally, the occurrence of surface or edge modes was

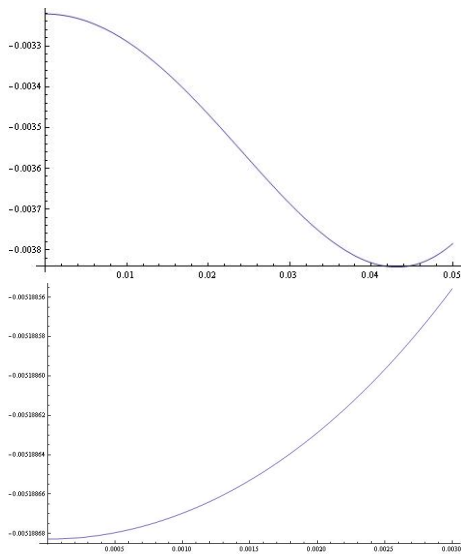


FIG. 4: Finite temperature effective potential \mathcal{V} as a function of σ in units of \sqrt{eB} : $\beta = 100/\sqrt{eB}$ and $\Omega = 0.0003\sqrt{eB}$ (top); $\beta = 43/\sqrt{eB}$ and $\Omega = 0.0001\sqrt{eB}$ (bottom).

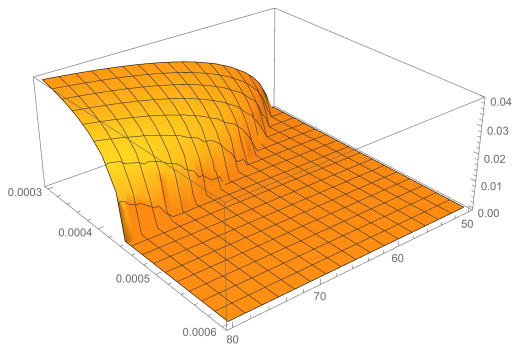


FIG. 5: Effective mass as a function of β and Ω in units of \sqrt{eB} at $T \neq 0$.

noted recently in [9]. We show in Appendix IX that they do not alter our current discussion for large N .

3. Dense state with $\Omega \neq 0$

For completeness, we now explore the effects of a finite chemical potential μ on the mass gap for $\bar{\psi}\psi$ pairing. Just as a caution, we note that a more complete treatment would require the inclusion of the competing $\psi\psi$ channel as well. However, we note that in leading order in $1/N_c$ the $\psi\psi$ channel is $1/N_c$ suppressed in comparison to the $\bar{\psi}\psi$ channel and can be ignored. With this in mind, the effect of a finite chemical potential follows from (82) through the substitution $\Omega(l + \frac{1}{2}) \rightarrow \mu + \Omega(l + \frac{1}{2})$, which we now briefly address.

In Fig. 7 we show the behavior of the effective potential

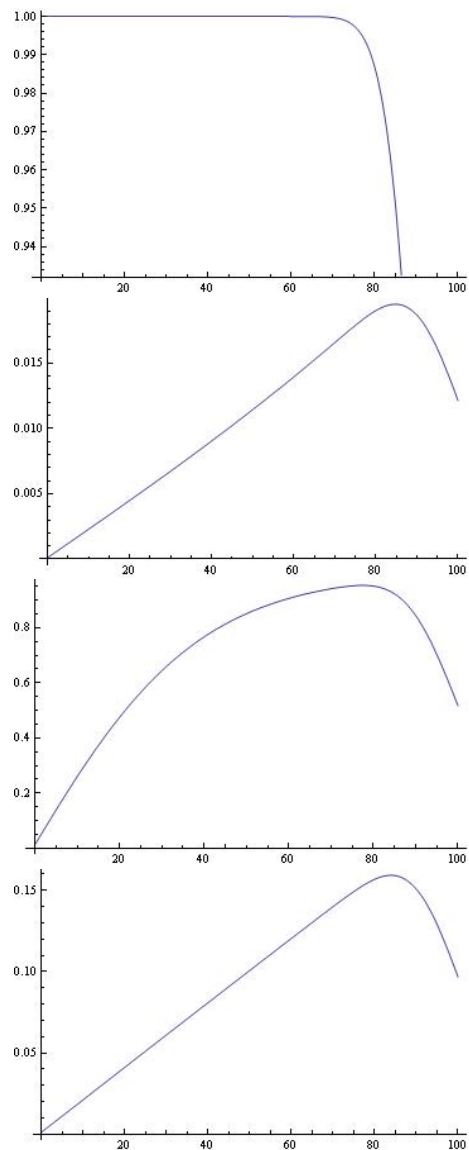


FIG. 6: The current density in the weak coupling regime with $g_r = 1$, as a function of $x = \frac{eBr^2}{2}$ in unit of $\frac{eB}{2\pi}$ at $T = 0$ and $\Omega = 0.0005$ (in unit of \sqrt{eB}) (first); $\beta = 100$, $\Omega = 0.0001$ (second); $\beta = 100$, $\Omega = 0.0005$ (third); $\beta = 40$, $\Omega = 0.0001$ (fourth)

\mathcal{V} for $\beta = 80/\sqrt{eB}$ and $\mu = 0.007/\sqrt{eB}$ as a function of σ in units of \sqrt{eB} . The top figure is for $\Omega = 0$ and the bottom figure is for $\Omega = 0.0003\sqrt{eB}$. The increase in the rotation causes the loss of the gapped solution. In particular, for $g_r = 1$ (weak coupling), $\beta = 80/\sqrt{eB}$ and $\Omega = 0$, the critical value is $\mu_c = 0.02\sqrt{eB}$, while for $\Omega = 0.0003\sqrt{eB}$, the critical value is $\mu_c = 0.007\sqrt{eB}$.

Finally and for completeness, we discuss in Appendix III the dense state with *negative* μ . Since the model under consideration can be viewed as an effective description of planar condensed matter systems [12], a negative

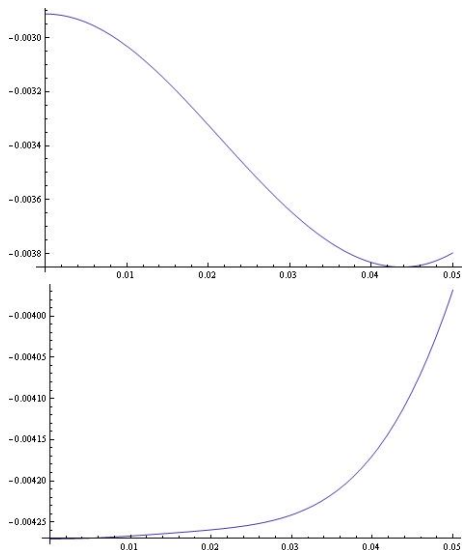


FIG. 7: Finite temperature effective potential $\mathcal{V}(\sigma)$ at $\beta = 80/\sqrt{eB}$ and $\mu = 0.007/\sqrt{eB}$ as a function of σ in units of \sqrt{eB} : $\Omega = 0$ (top) and $\Omega = 0.0003\sqrt{eB}$ (bottom)

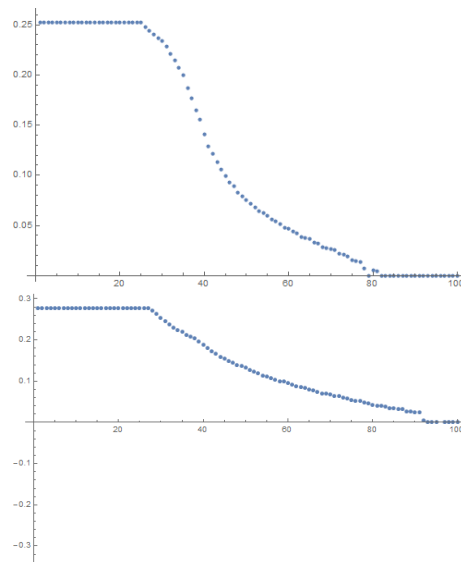


FIG. 8: Mass gap σ/Λ in the strong coupling regime with $g_r = -4$, as a function of $\Omega/(10^{-4}\Lambda)$ for $\Lambda/\sqrt{eB} = 5$ (top) and $\Lambda/\sqrt{eB} = 3$ (bottom).

chemical potential is experimentally accessible.

B. Strong coupling regime

In the opposite regime of strong coupling with $g > g_c$, a mass gap also forms. In the regime where the ratio $\frac{\Lambda}{\sqrt{eB}}$ is large and $g > g_c$ or $g_r < 0$, the minimum of the effective potential is now controlled by the first and third contributions in (28) namely

$$\frac{\mathcal{V}_0}{N_c} \approx -\frac{\Lambda\sigma^2}{2\pi|g_r|} + \frac{\sigma^3}{3\pi} \quad (36)$$

with a mass gap $\bar{\sigma} = \Lambda/|g_r|$. For $\sqrt{eB}/\Lambda < 1$, the leading contribution shifts the mass and the scalar condensate quadratically,

$$\frac{\langle \bar{\psi}\psi \rangle_B}{\langle \bar{\psi}\psi \rangle_0} - 1 \approx \frac{(eB)^2}{12(\Lambda/g_r)^4} \quad (37)$$

We note that the ratio of the mass gap to the LL gap $\bar{\sigma}/\sqrt{eB}$ can be very large. Therefore, the critical Ω_c for which the mass gap can be depleted is much larger in strong coupling than in weak coupling. For fixed Ω , the mass $\bar{\sigma}$ decreases as the ratio Λ/\sqrt{eB} decreases. For instance, for $g_r = -4$ and $\Lambda/\sqrt{eB} = 5$, $\Omega_c \approx 0.008\Lambda$, but for $\Lambda/(\sqrt{eB}|g_r|) = 3$, $\Omega_c \approx 0.009\Lambda$. In Fig. 9 we show the behavior of the mass gap for strong coupling with $g_r = -4$ versus σ in units of Λ as a function of Ω expressed in units of $\Lambda/10^4$. The top figure is for $\Lambda/\sqrt{eB} = 5$ and the bottom figure is for $\Lambda/\sqrt{eB} = 3$.

IV. DIRAC FERMIONS IN 1+3

The extension of the previous analysis to 1+3 dimensions for free Dirac fermions is straightforward. In Appendix IV we detail the rotating wavefunctions in the presence of a magnetic field, for the free case. The interacting case is more challenging for say the case of QCD which is strongly coupled and gapped in the vacuum. Below, we will focus on the combined effects of a rotation and magnetic field on the QCD chiral condensate in the spontaneously broken phase using mesoscopic arguments, and leading order chiral perturbation.

A. Free left currents

We now extend the analysis for the left or L-currents to show the generic nature of the observations made in 1 + 2 dimensions above. From Appendix IV, the L-wavefunctions in 1 + 3 dimensions take the simplifying form

$$\begin{aligned} u_L(n=0) &= v_L(n=0) = \sqrt{\frac{\tilde{E}-p}{2\tilde{E}}}(f_{0,m},0) \\ u_L(n,m) &= \frac{1}{\sqrt{2\tilde{E}(\tilde{E}+p)}}(\sqrt{2eBn}f_{nm}, (\tilde{E}+p)f_{n-1,m}) \\ v_L(n,m) &= \frac{1}{\sqrt{2\tilde{E}(\tilde{E}+p)}}(\sqrt{2eBn}f_{nm}, -(\tilde{E}+p)f_{n-1,m}) \end{aligned} \quad (38)$$

The left particle density at the origin is

$$\begin{aligned}
& \frac{1}{N} n_L(0) = \\
& + \int_{-\infty}^0 \frac{dp}{2\pi} (n_F(-p - \mu_{00}) - n_F(-p + \mu_{00})) \\
& + \sum_{n=1}^{\infty} \int_{-\infty}^{\infty} \frac{dp}{4\pi} (n_F(E_n - \mu_{00}) + n_F(E_n - \mu_{10})) \\
& - \sum_{n=1}^{\infty} \int_{-\infty}^{\infty} \frac{dp}{4\pi} (n_F(E_n + \mu_{00}) + n_F(E_n + \mu_{10}))
\end{aligned} \tag{39}$$

while the current density at the origin is

$$j_L^3(0) = N \left(J_{L,0}^3 + \sum_{n=1} J_{L,n}^3 \right) \tag{40}$$

with

$$\begin{aligned}
J_{L,0}^3 &= - \int_{-\infty}^0 \frac{dp}{2\pi} (n_F(-p - \mu_{00}) - n_F(-p + \mu_{00})) \\
&= - \frac{\Omega}{4\pi} - \frac{\mu_L}{2\pi} \\
J_{L,n}^3 &= - \sum_{n=1}^{\infty} \int_{-\infty}^{\infty} \frac{dp}{4\pi} (n_F(E_n - \mu_{00}) - n_F(E_n - \mu_{10})) \\
&+ \sum_{n=1}^{\infty} \int_{-\infty}^{\infty} \frac{dp}{4\pi} (n_F(E_n + \mu_{00}) - n_F(E_n + \mu_{10}))
\end{aligned} \tag{41}$$

with $\mu_{00} = \frac{\Omega}{2} + \mu_L$ and $\mu_{10} = -\frac{\Omega}{2} + \mu_L$. For small B and zero μ_L , the summation in (40) gives

$$\sum N f(\sqrt{p^2 + 2gBn}) \rightarrow \int \frac{kdk}{2\pi} f(\sqrt{p^2 + k^2}) \tag{42}$$

This reproduces the known result at $B = 0$ [1]

$$- \frac{T\Omega}{12\pi^2} - \frac{(\Omega + 2\mu_L)^3 + (\Omega - 2\mu_L)^3}{96\pi^2} \tag{43}$$

While the current density at the origin reproduces the expected result, the distribution of the current density in the radial direction is not homogeneous. Indeed, the centrifugation causes it to peak at the edge as in 1 + 2 dimensions. This is readily seen from the contribution of the LLL which can be worked out explicitly with the result

$$J_{Ln=0}^3 = - \frac{N}{2\pi} \sum_{m=0} e^{-\frac{eBr^2}{2}} \left(\frac{eBr^2}{2} \right)^m \frac{(m + 1/2)\Omega + \mu_L}{m!} \tag{44}$$

The sum can be performed exactly with the result

$$J_{Ln=0}^3(r) = \frac{N}{2\pi} \left(\mu_L + \Omega \left(\frac{1}{2} + \pi N r^2 \right) \right) \tag{45}$$

The *centrifugal effect* causes the current density to peak at the edge of the rotational plane in 1 + 3 dimensions.

A possible application of this phenomenon maybe in current heavy ion collisions at collider energies such as RHIC and LHC. Indeed, for semi-central collisions both the rotational (orbital) and electric magnetic fields are sizable with $\Omega \sim eB \sim m_\pi$ which may induce partonic densities of the type (45) that are largely deformed in the transverse plane. While the rotation and magnetic fields tend to separate the partonic charges in concert along the rotational axis, the centrifugation causes this separation to peak in the orthogonal direction where the observed particle flow is more important. If true, this effect should be seen as an enhancement of v_4 in the charged particle flow.

B. Number of free left particles

As we noted in 1 + 2 dimensions, the number of free left particles increases in 1 + 3 dimensions due to the sinking of the particle LLL in the Dirac sea. More explicitly, we have

$$\begin{aligned}
n_L &= \int dx dy \langle : \bar{\psi}_L \gamma^0 \psi_L : \rangle \\
&= \sum_m \int_{-\infty}^0 \frac{dp}{2\pi} (n_F(-p - \mu_m) - n_F(-p + \mu_m)) \\
&+ \sum_{n=1,m} \int_{-\infty}^{\infty} \frac{dp}{2\pi} (n_F(E_n - \mu_{nm}) - n_F(E_n + \mu_{nm}))
\end{aligned} \tag{46}$$

Here $\mu_{nm} = (m - n + \frac{1}{2})\Omega + \mu_L$ and $E_n = \sqrt{p^2 + 2eBn}$. The flowing left current along the rotational-magnetic axis is

$$\begin{aligned}
j_L^3 &= \int dx dy \langle \bar{\psi}_L \gamma^3 \psi_L \rangle \\
&= - \sum_m \int_{-\infty}^0 \frac{dp}{2\pi} (n_F(-p - \mu_m) - n_F(-p + \mu_m)) \\
&= - \frac{1}{2\pi} \sum_{m=0}^N \left(m + \frac{1}{2} \right) \Omega + \mu_L \\
&= - \frac{\Omega}{2\pi} \left(N + \frac{N^2}{2} \right) - \frac{\mu_L N}{2\pi}
\end{aligned} \tag{47}$$

The first contribution in (47) was noted in [5, 7]. (46-47) generalize to arbitrary 1 + d dimensions. In particular, for $\mu_L = 0$

1. Diffusion in the vacuum

$$n_{L0} = \frac{2^{\frac{d-3}{2}} V_{d-2}}{(2\pi)^{d-2}} \text{sgn}(\Omega) |\Omega|^{d-2} \sum_{m=1}^N \left(m + \frac{1}{2}\right)^{d-2} \quad (48)$$

with the volume $V_{d-2} = \pi^{\frac{d}{2}-1} / \Gamma(\frac{d}{2})$.

C. Relation to anomalies

These observations can be used to generalize (49) to arbitrary $1 + d = 2n$ dimensions. Consider the case with non-vanishing and non-parallel magnetic fields $B_{2k,2k+1} \neq 0$ with $1 \leq k \leq n-3$. The general anomaly induced chiral magnetic effect for the left current is [10]

$$J_{L\mu L}^{2n-1} = -\frac{\mu_L}{2\pi} \left(\frac{e}{2\pi}\right)^{n-1} B_{12} B_{34} \dots B_{2n-4,2n-3} \quad (49)$$

We now observe from (45) that the role of the rotation is to tag to μ_L in $2n = 4$ dimensions as

$$\frac{eB}{2\pi} \left(\mu_L + \Omega \left(\frac{1}{2} + \pi N r^2 \right) \right) \equiv \mu_L \frac{eB}{2\pi} + \Omega J(r) \quad (50)$$

The anomalous result (49) relates to the rotationally induced current by a similar substitution in $2n$ dimensions, namely

$$J_{L\Omega}^{2n-1}(r) = -\frac{1}{2\pi} \left(\frac{e}{2\pi}\right)^{n-2} B_{12} B_{34} \dots B_{2n-6,2n-5}(\Omega, J(r)) \quad (51)$$

where $J(r)$ refers to the current spin density in the radial direction within the $2n-4, 2n-3$ plane

$$J_{2n-4,2n-3}(r) = \frac{eB_{2n-4,2n-3}}{2\pi} \left(\frac{1}{2} + B_{2n-4,2n-3} \frac{r^2}{2} \right) \quad (52)$$

The rotational contribution to the current density (51) in $2n$ dimensions is related to the chiral magnetic effect (49) in $2n-2$ dimensions.

D. Interacting Dirac fermions in 1+3

Now we consider the case of interacting Dirac fermions in the context of QCD in 1+3 dimensions at strong coupling. In this regime, a mass gap forms and chiral symmetry is spontaneously broken with a triplet of charged Goldstone modes. They play the role of diffusons in the vacuum [13]. We will not quantify these statements for the QCD chiral condensate.

The spontaneous breaking of the symmetry is manifest though a finite scalar condensate, which in the chiral limit relates to the quark return probability in proper time τ as [13]

$$\langle \bar{\psi}\psi \rangle_{0,0} = -\lim_{m \rightarrow 0} \lim_{V_4 \rightarrow \infty} \frac{1}{V_4} \int_0^\infty P(0, \tau) d\tau \quad (53)$$

with

$$P(0, \tau) = \left\langle \left| u^+(\tau)u(0) + d^+(\tau)d(0) \right|^2 \right\rangle \quad (54)$$

for 2 light u, d flavors. The averaging in (54) is over the QCD vacuum in Euclidean 4-dimensional space. In the absence of magnetism, the vacuum is isospin symmetric and the correlator in (54) is dominated by the lightest Goldstone modes $\pi^{0,\pm}$

$$P(0, \tau) = 2(P_0(0, \tau) + P_\pm(0, \tau)) \approx \sum_Q e^{-\tau D(0,0)Q^2} \quad (55)$$

The sum is over the pions or diffusons with momenta $Q_\mu = n_\mu 2\pi/L$ in a periodic $V_4 = L^4$ Euclidean box. The vacuum diffusion constant is $D(0,0) = 2F_\pi^2 / |\langle \bar{\psi}\psi \rangle_{0,0}|$ [13].

2. Diffusion with $B, \Omega \neq 0$

Under rotations all $\pi^{0,\pm}$ are affected by centrifugation, while only the π^\pm are affected by magnetism. As a result, the squared and Euclideanized pion spectra are

$$\begin{aligned} \lambda_0^2 &= p_r^2 + p_3^2 + (p_4 + i\Omega l)^2 + m_\pi^2 \\ \lambda_\pm^2 &= eB(2n+1) + p_3^2 + (p_4 + i\Omega l)^2 + m_\pi^2 \end{aligned} \quad (56)$$

Each chargeless mode carries $l = 0, \pm 1, \dots$, while each charged mode is in a LL n where $-n \leq l \leq N-n$ with degeneracy N . Note that the rotational energy shift in Euclidean space is purely imaginary. The change in each of the return probabilities in (55) following from (56) is

$$\begin{aligned} P_0(\Omega, \tau) &= \sum_{n_r, n_3, n_4} \sum_{l=-\infty}^{+\infty} \\ &\times e^{-\tau D(\Omega, B)(p_r^2 + p_3^2 + (p_4 + i\Omega l)^2 + m_\pi^2)} \\ P_\pm(B, \Omega, \tau) &= \sum_{n_3, n_4} \sum_{n=0}^N \sum_{-n \leq l \leq N-n} \\ &\times e^{-\tau D(\Omega, B)(eB(2n+1) + p_3^2 + (p_4 + i\Omega l)^2 + m_\pi^2)} \end{aligned} \quad (57)$$

with $p_{3,4} = n_{3,4}(2\pi/L)$ in an Euclidean box of 4-volume chosen cylindrical with $V_4 \rightarrow \pi R^2 L^2$ and the causal constraint $\Omega R < 1$. In general, in the rotating vacuum with magnetism the diffusion constant $D(\Omega, B)$ is Ω, B dependent.

The change in the quark return probability is the change in the charged diffuson modes and is captured by the difference

$$I = \int_0^\infty [P(\Omega, B, \tau) - P(0, 0, \tau)] d\tau \quad (58)$$

In the chiral limit, replacing the sums over free momenta by integrals allows to get rid of the explicit Ω dependence in (57) by shifting p_4 . So the dependence on Ω, B in P_0 is only through $D(\Omega, B)$. Clearly, in the absence of B a rotation Ω alone cannot change the return probability, and therefore the chiral or scalar condensate as the vacuum is rotationally symmetric. This is not the case in the presence of an externally fixed magnetic field B as rotational symmetry is broken. Indeed, the LL dependence in P_\pm does not drop but can be resummed exactly with the result

$$I = \frac{eBV_4}{16\pi^2 D} \int_0^\infty \left(\frac{1}{z \sinh z} - \frac{1}{z^2} \right) dz = -\frac{\ln 2}{16\pi^2} \frac{eBV_4}{D(\Omega, B)} \quad (59)$$

Using the value of the diffusion constant we arrive at

$$\frac{\langle \bar{\psi}\psi \rangle_{\Omega, B}}{\langle \bar{\psi}\psi \rangle_{0,0}} - 1 = \frac{\ln 2}{16\pi^2} \frac{eB}{F_\pi^2} \frac{D(0,0)}{D(\Omega, B)} \quad (60)$$

For $\Omega = 0$ and $B \neq 0$, (60) is in agreement with chiral perturbation theory in leading order [14]. This linear magnetic catalysis is supported by lattice simulations [15].

(60) is the analogue of (37) in 1 + 2 dimensions at strong coupling, with the difference that it grows linearly not quadratically. The quadratic growth follows from the absence of charged Goldstone modes. As indicated earlier, in 1+2 dimensions the gapped phase is a BKT phase not a Goldstone phase. We now give an independent determination that fixes $D(\Omega, B)$ in (60).

3. Vacuum pion fluctuations and condensation

In leading order in the pion interactions, the unsubtracted vacuum energy density for charged pions at finite Ω, B and zero temperature is the sum of a purely B dependent contribution $\mathcal{E}_{\pi B}$ and a mixed B, Ω dependent contribution $\mathcal{E}_{\pi\Omega}$

$$\mathcal{E}_\pi(\Omega, B) = \mathcal{E}_{\pi B} + \mathcal{E}_{\pi\Omega} \quad (61)$$

Now we note that $\mu_l = \Omega l$ acts as a finite pion chemical potential on the rotating pion spectrum at finite B , in much the same way as noted for fermions in [1, 7, 8]. Therefore, when $\mu_N = N\Omega$ exceeds the π^+ effective mass $m_0 = \sqrt{eB + m_\pi^2}$, the π^+ will Bose condense in the lowest energy state characterized by $p = 0$ and $n = 0, m = N$. Other arrangements of the condensed π^+ in the LL are also possible, for instance by arranging them in layers with different orbital assignment in bulk, but they cost more Coulomb energy. The condensation of π^- requires Ω, B antiparallel.

Now, let \mathbf{n} be the number of condensed π^+ per unit length L along the rotational axis. The energy of the pion π^\pm vacuum fluctuations and the pion π^+ condensate are respectively

$$\begin{aligned} \mathcal{E}_{\pi B} &= 2 \frac{N}{S} \int_{-\infty}^{+\infty} \frac{dp}{2\pi} \sum_{n=0}^{\infty} \frac{1}{2} \epsilon_n(p) \\ \mathcal{E}_{\pi\Omega} &= -\frac{\mathbf{n}}{S} (N\Omega - m_0) + c_N \frac{\mathbf{n}^2}{S} \end{aligned} \quad (62)$$

with $\epsilon_n^2(p) = p^2 + m_n^2$ and $m_n^2 = (2n+1)eB + m_\pi^2$. Here c_N is the Coulomb factor stemming from the Coulomb repulsion in the condensed droplet of π^+ by centrifugation. The 2-dimensional charge distribution in this state is given by $\rho_N(\tilde{x}) = |f_{0N}(x, y)|^2$ which is valued in $S = \pi R^2$. The condensate lies at the edge of the rotational plane with a Coulomb factor

$$c_N = \frac{1}{2L} \int_{L \times S} d^3x d^3x' \rho_N(\tilde{x}) \frac{1}{|x - x'|} \rho_N(\tilde{x}') \quad (63)$$

In the large N limit, we can approximate this distribution by a uniform radial distribution within the area $N - \sqrt{N} \leq \frac{eBr^2}{2} \leq N + \sqrt{N}$ with total charge 1. It follows that the Coulomb factor is

$$c_N \approx \frac{1}{12\pi\sqrt{N}} \quad (64)$$

The condensate density \mathbf{n} is fixed by minimizing the energy density $\mathcal{E}_{\pi\Omega}$ in (62), with the result

$$\mathbf{n} = \theta(N\Omega - m_0) \frac{N\Omega - m_0}{2c_N} \quad (65)$$

$$\approx 6\pi\sqrt{N}(N\Omega - m_0)\theta(N\Omega - m_0) \quad (66)$$

for which the energy density in (62) is

$$\mathcal{E}_{\pi\Omega} \rightarrow -\frac{3\pi\sqrt{N}}{S} (N\Omega - m_0)^2 \theta(N\Omega - m_0) \quad (67)$$

For fixed LL, the π^+ particle states with $|\Omega l| < m_n$ Bose condense under the double effects of Ω, B . This condensation is for bosons, what the shift to the Dirac sea of

positive energy states in the LLL is for fermions. For $eB = 0.1 m_\pi^2$, and $N = 1000$, the threshold for developing non-zero \mathbf{n} is $\Omega_{\min} = 0.001 m_\pi$. For $\Omega = 0.0015 m_\pi$, we have $\mathbf{n} = 268 m_\pi$, and for $\Omega = 0.002 m_\pi$, we have $\mathbf{n} = 566 m_\pi$.

In leading order, the chiral condensate follows from (61-62) as

$$\langle \bar{\psi}\psi \rangle_{\Omega,B} = \frac{\partial \mathcal{E}_\pi(\Omega, B)}{\partial m} \quad (68)$$

modulo vacuum renormalization. Using the GOR relation $m_\pi^2 F_\pi^2 = -m \langle \bar{\psi}\psi \rangle_{0,0}$ in the absence of Ω, B , we can trade the derivative in (68) with the derivative with respect to the pion mass. For the Ω independent pion contribution in (61) we explicitly have

$$\frac{\partial \mathcal{E}_{\pi B}}{\partial m} = \frac{\langle \bar{\psi}\psi \rangle_{0,0}}{(4\pi F_\pi)^2} \int ds \frac{eB e^{-sm_\pi^2}}{s \sinh(eBs)} \quad (69)$$

The corresponding shift in the chiral condensate for $\Omega = 0$ but finite B is

$$\frac{\langle \bar{\psi}\psi \rangle_B}{\langle \bar{\psi}\psi \rangle_{0,0}} - 1 = \frac{\ln 2}{16\pi^2} \frac{eB}{F_\pi^2} \quad (70)$$

in agreement with (60). A rerun of the same arguments for the Ω dependent contribution in (62) gives for the corresponding change of the chiral condensate caused by the rotation

$$\begin{aligned} & \frac{\langle \bar{\psi}\psi \rangle_\Omega}{\langle \bar{\psi}\psi \rangle_{0,0}} \\ &= \frac{3eB}{2F_\pi^2 \sqrt{N}} \frac{(m_0 - N\Omega)}{m_0} \theta(N\Omega - m_0) \end{aligned} \quad (71)$$

The net shift of the chiral condensate due to both the magnetic field and the rotation for which a pion condensation occurs is

$$\begin{aligned} & \frac{\langle \bar{\psi}\psi \rangle_{\Omega,B}}{\langle \bar{\psi}\psi \rangle_{0,0}} - 1 = \\ & \frac{1}{2} \frac{eB}{F_\pi^2} \left(\frac{\ln 2}{8\pi^2} - \frac{3}{\sqrt{N}} \left(\frac{N\Omega}{m_0} - 1 \right) \theta(N\Omega - m_0) \right) \end{aligned} \quad (72)$$

in leading order in the pion interaction. The change of the chiral condensate under the combined effects of a magnetic field and a rotation was initially suggested using arguments from random matrix theory and anomalies [4, 16]. It was clarified and detailed in the context of the NJL model in [6, 7]. For $N\Omega \gg \sqrt{eB}$ and retaining only the LLL in (72) gives for the total shift in the chiral condensate under the dual effects of Ω, B

$$\frac{\langle \bar{\psi}\psi \rangle_{\Omega,B}}{\langle \bar{\psi}\psi \rangle_{0,0}} - 1 \approx \frac{1}{2} \frac{eB}{F_\pi^2} \left(\frac{\ln 2}{8\pi^2} - \frac{3\Omega\sqrt{N}}{m_0} \right) \quad (73)$$

(73) fixes the ratio of the diffusion constants in (60). The effect of the rotation is to inhibit the so-called magnetic catalysis as emphasized in [7]. Note that (73) is of order N_c^{-1} and would be missed in an effective calculation with constituent quarks such as in the NJL model in the leading loop or N_c^0 approximation. (73) suggests that a rotation $\Omega_\star \sim m_0/\sqrt{N}$ compensates the increase induced by the magnetic field. In this approximation, the chiral condensate vanishes for

$$\Omega_c \approx \frac{m_0}{3\sqrt{N}} \left(\frac{\ln 2}{8\pi^2} + \frac{2F_\pi^2}{eB} \right) \quad (74)$$

4. Pion superfluid in heavy-ion collisions

Current heavy ion collisions at collider energies in non-central collisions involve large angular momenta in the range $10^3 - 10^5 \hbar$ [17, 18]. Recently, STAR reported a large vorticity with $\Omega \sim (9 \pm 1) 10^{21} s^{-1} \sim 0.05 m_\pi$, by measuring the global polarization of Λ and $\bar{\Lambda}$ in off central AuAu collisions in the Beam Energy Scan program [19]. Assuming that at chemical freeze-out, $R \sim 10$ fm and $eB \sim m_\pi^2$, this would translate to a LL degeneracy $N = eBR^2/2 \sim (m_\pi \times 10 \text{ fm})^2 \sim 100/4$ and a rotational chemical potential $\mu_N = N\Omega \sim 1.25 m_\pi$. From the hadro-chemistry analysis, the pion chemical potentials at freeze-out are typically $\mu_f \sim 0.5 m_\pi$ at RHIC, and $\mu_f \sim 0.70 m_\pi$ at the LHC. With the rotation at finite B , they would translate to $\mu_\pi = \mu_N + \mu_f \sim 1.75 m_\pi$ and $1.96 m_\pi$ respectively. Since the threshold of the LLL for the pion energy is $\sqrt{2} m_\pi$ (ignoring the shift in the pion mass caused by the drop in the chiral condensate), it is possible for the charged pion condensation mechanism to take place, in the form of a rotating pion super-current at the edge of the fire ball.

The condensation involves few hundred pions. Indeed, for an estimate we can separate the superfluid phase from the normal thermal phase. At finite T, μ_f , the pion superfluid phase is described by the partition function

$$\mathbb{Z} = \sum_{p=0}^{\infty} e^{p \frac{N\Omega + \mu_f - m_0}{T} - \frac{p^2}{12\pi\sqrt{N}TL}} \quad (75)$$

with the superfluid energy fixed by (62). The mean number of condensed π^+ follows as

$$\mathbb{N}_{\pi^+} = \sum_{p=0}^{\infty} \frac{p}{\mathbb{Z}} e^{p \frac{N\Omega + \mu_f - m_0}{T} - \frac{p^2}{12\pi\sqrt{N}TL}} \quad (76)$$

For $L \sim 10$ fm, $eB \sim m_\pi^2$ and $N \approx 25$, we show in Fig. 9 the average number of condensed π^+ for temperatures in the range $0.5 m_\pi \leq T \leq 1.5 m_\pi$ and rotations in the range $0.02 m_\pi \leq \Omega \leq 0.05 m_\pi$. The upper plot is for a pion chemical potential at freeze-out $\mu_f = 0.5 m_\pi$, and the lower plot is for $\mu_f = 0.8 m_\pi$. As Ω exceeds the critical Ω_{\min} , the number of π^+ increases dramatically to few hundreds with a very weak dependence on the temperature. Clearly, such an effect can only take place in current heavy ion collisions, if the induced magnetic field eB persists with considerable strength in the freeze-out region.

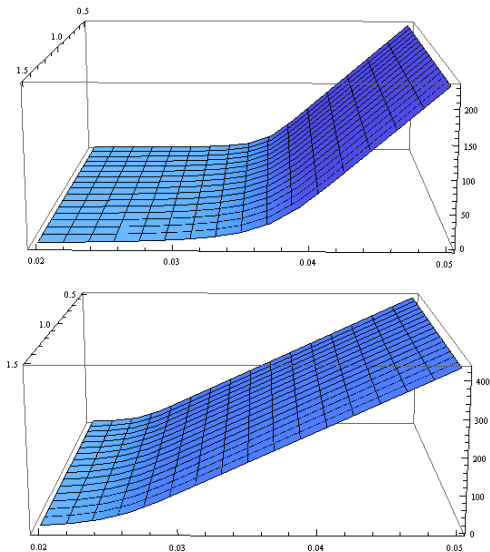


FIG. 9: The mean number of superfluid pions (76) in the range $0.5 m_\pi \leq T \leq 1.5 m_\pi$ and $0.02 m_\pi \leq \Omega \leq 0.05 m_\pi$, for $\mu_f = 0.5 m_\pi$ (top) and $\mu_f = 0.8 m_\pi$ (bottom).

V. CONCLUSIONS

We analyzed the combined effects of a rotation and a magnetic field on free and interacting Dirac fermions in 1+2 dimensions. Our results show that the rotation causes massless positive states in the LLL to sink into the Dirac sea, followed by an increase in the density of particles. The scalar density of particles does not change in the free case, but is modified in the interacting case. These results strengthen our earlier observation that an increase in the density of composite fermions in the quantum Hall effect at half filling under rotation would signal their Dirac nature [4]. They may also be of relevance to planar condensate matter systems when subject to a parallel rotation plus a magnetic field.

We showed that the mechanism behind the sinking of the LLL for free Dirac fermions, holds in any dimension, leading to a finite increase in the density of particles that is related to anomalies. For QCD in the spontaneously

broken phase with Dirac fermions, this mechanism manifests itself in a novel way through the condensation of charged pions. We used this observation to derive an exact result for the shift in the chiral condensate in leading order in the pion interaction.

On a more speculative way in QCD, the charged separation caused by the dual combination of a rotation parallel to a magnetic field, may impact on the flow of charged particles in semi-central collisions of heavy ions at present collider energies, provided that the magnetic field is still strong in the freeze-out region. While both the rotation and the magnetic field separate charges along the rotational axis as known through the standard chiral vortical and magnetic effect, the combined effect causes them to centrifuge. The resulting charge separation is quadrupolar as opposed to polar with some consequences for the charged particle flow. Also, the possibility of an induced and coherent charge accumulation by rotation in a magnetic field, whether in the form of partons or pions, may affect the fluctuations in the charge and pion number, the transport coefficients such as the viscous coefficients, and potentially the electromagnetic emissivities in the prompt and intermediate part of the collision, especially their distribution and flow in the low mass region. These issues are worth further investigations.

VI. ACKNOWLEDGEMENTS

We thank Edward Shuryak for a discussion, and Maxim Chernodub for bringing his work to our attention. This work was supported in part by the U.S. Department of Energy under Contract No. DE-FG-88ER40388.

VII. APPENDIX I: RANGE OF l

To better understand the nature of the range in the orbital angular momentum l for each LL, we recall that for $l \geq 0$ the wavefunction is typically of the form

$$z^l e^{-\frac{eBr^2}{4}} L_n^l(eBr^2/2) \quad (77)$$

The requirement that (77) stays within the area $S = \pi R^2$ implies that $l + n < N$, meaning that both $l, n < N$. Conversely, for $l < 0$ the wavefunctions are of the form

$$z^{|l|} e^{-\frac{eBr^2}{4}} L_{n-|l|}^{|l|}(eBr^2/2) \quad (78)$$

which requires $n \leq N$. But for this case, we always have $n \geq -l$. These observations imply that the orbital angular momentum is bracketed with $-n \leq l \leq N - n$. This range of l helps keep the angular shift Ωn smaller than the magnetic shift \sqrt{eBn} for large n . Indeed, this requirement together with the causality bound $\Omega R < 1$, implies that

$$\sqrt{2eBn} - \Omega|l| \geq \frac{1}{R}(\sqrt{4N^2} - N) \approx \sqrt{NeB} \quad (79)$$

VIII. APPENDIX II: ALTERNATIVE \mathcal{V}_T

The one-loop finite temperature contribution to the effective potential relates to the scalar condensate through

$$\frac{\partial \mathcal{V}_T}{\partial \sigma} = - \int d^2x \langle \bar{\psi} \psi \rangle |_{\beta}. \quad (80)$$

Using the quantized fields (8) and the proper time construction, we have

$$\begin{aligned} \frac{\partial \mathcal{V}_T}{\partial \sigma} &= -4\sigma \int \frac{d\omega}{2\pi} \sum_l f_F(\omega, l) \\ &\times \text{Im} \int_0^\infty idse^{-is(\omega^2 - \sigma^2 - i\epsilon)} \left(\sum_{n_{min}} (2 - \delta_{n,0}) e^{i2eBns} \right) \end{aligned} \quad (81)$$

For positive l , the constraint is $l \leq N - n$, thus the upper bound for l is N and for a given l the upper bound for n is $N - l$. For negative l , we also have $|l| \leq N$ and $|l| \leq n \leq N$. Thus, the summation over n gives for positive l

$$\frac{1 + e^{2ieBs}}{1 - e^{2ieBs}} - 2 \frac{e^{2ieBs(N-l)}}{1 - e^{2ieBs}} \quad (82)$$

Since we have

$$f_F(\omega, l) = \frac{\theta(\omega)}{e^{\beta(\omega - \Omega(l+1/2) - \mu)}} + \frac{-\theta(\omega)}{e^{\beta(-\omega + \Omega(l+1/2) + \mu)}} \quad (83)$$

it is clear that $|f_F| \leq 2$. Thus the summation of the second term in (82) is of order

$$\frac{1 - e^{2ieB(Ns)}}{1 - e^{2ieBs}} \quad (84)$$

After analytical continuation to the imaginary axis, this contribution vanishes in the thermodynamical limit. The only contribution is to the residue which is l -independent. For negative l we have

$$\frac{e^{2iNeBs} - e^{2iNeBs|l|}}{1 - e^{2ieBs}} \quad (85)$$

After analytic continuation, neither the residue nor the integrand part survive. With all in mind, the result is now

$$\begin{aligned} \frac{\partial \mathcal{V}_T}{\partial \sigma} &= -4\sigma \int \frac{d\omega}{2\pi} \sum_{l=0}^N f_F(\omega, l) \\ &\times \text{Im} \int_0^\infty idse^{-is(\omega^2 - \sigma^2 - i\epsilon)} \\ &\times \left(\frac{1 + e^{2ieBs}}{1 - e^{2ieBs}} - 2 \frac{e^{2ieBs(N-l)}}{1 - e^{2ieBs}} \right) \end{aligned} \quad (86)$$

For $\omega^2 - \sigma^2 \leq 0$, the analytical continuation of the integrand to the positive imaginary axis yields zero imaginary part. For $\omega^2 - \sigma^2 \geq 0$ the analytical continuation of the first and second contributions to the negative and positive real axis respectively, yield adding residues with a net imaginary part. The result is

$$\begin{aligned} \frac{\partial \mathcal{V}_T}{\partial \sigma} &= -4\sigma \int \frac{d\omega}{eB} \theta(\omega^2 - \sigma^2) \sum_{l=0}^N f_F(\omega, l) \\ &\times \left(\frac{1}{2} + \sum_{n=1}^\infty \cos\left(\frac{\pi n}{eB}(\sigma^2 - \omega^2)\right) \right) \end{aligned} \quad (87)$$

which integrates to

$$\begin{aligned} \mathcal{V}_T &= \int d\omega \sum_{l=0}^N f_F(l, \omega) \theta(\omega^2 - \sigma^2) \\ &\times \left(\left(\frac{\omega^2 - \sigma^2}{eB} \right) + \frac{2}{\pi} \sum_{n=1}^\infty \frac{\sin\left(\frac{\pi n}{eB}(\omega^2 - \sigma^2)\right)}{n} \right) \end{aligned} \quad (88)$$

Through a change of variable, we can recast each l -contribution in (88) in the form

$$\begin{aligned} &\int f_F(l, \omega) \theta(\omega^2 - \sigma^2) \frac{\omega^2 - \sigma^2}{eB} \\ &- \frac{2}{\pi} \sum_{n=0}^\infty \int_{\omega^2 - \sigma^2 \geq 2eBn}^{\omega^2 - \sigma^2 \leq 2eB(n+1)} f_F(\omega) \frac{\frac{\pi(\omega^2 - \sigma^2)}{eB} - (2n+1)\pi}{2} \end{aligned} \quad (89)$$

By partial integration we found that the first term cancels the last term, with only boundary terms left. The final result for the thermal contribution to the effective potential takes the canonical form

$$\mathcal{V}_T = \frac{1}{\beta} \sum_{l=N}^{\infty} \sum_{n=0}^{\infty} \sum_{j=1, -1} \ln(1 + e^{-\beta(E_n - j(\mu + \Omega(l + \frac{1}{2})))}) \quad (90)$$

This result is equivalent to (25) in the thermodynamical limit.

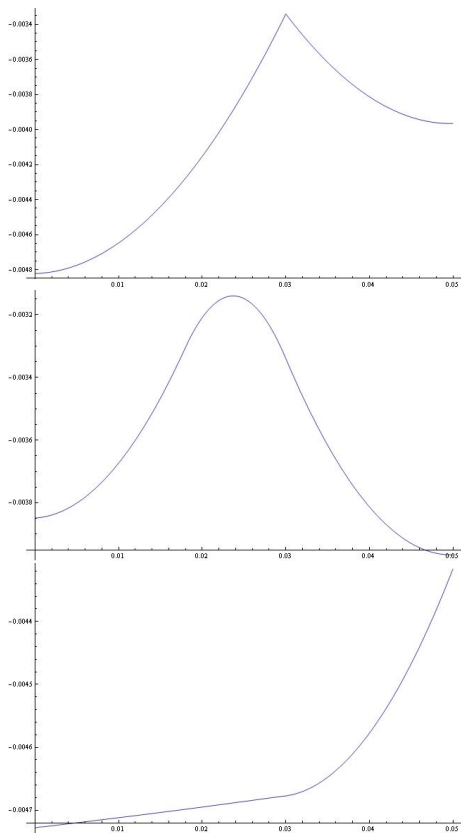


FIG. 10: Effective potential $\mathcal{V}(\sigma)$ at $T = 0$ and $\mu = -0.031/\sqrt{eB}$ in units of \sqrt{eB} : $\Omega = 0$ (top); $\Omega = 0.00012\sqrt{eB}$ (middle); and $\Omega = 0.001\sqrt{eB}$ (bottom).

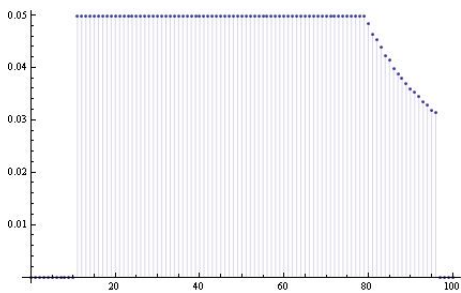


FIG. 11: Effective mass at $T = 0$ and $\mu = -0.03\sqrt{eB}$ in units of \sqrt{eB} as a function of Ω in units of $10^{-5}\sqrt{eB}$

IX. EDGE MODES IN 1+2

Recently, it was noted in [9] that for a negative fermion mass and when the boundary condition at the luminal radius R was enforced (for example through an MIT bag boundary condition, see also [20]), there is one imaginary solution to the radial wave number $k_{\perp} = \sqrt{E^2 - M^2}$ for each angular momentum m (in the infinite area case $k_{\perp}^2 = 2eBn$). These solutions were referred to as edge modes as they peak near the edge in the absence of a

magnetic field. For a finite magnetic field, the corresponding wave function reads

$$e^{-\frac{eBr^2}{4}} r^m e^{im\phi} {}_1F_1\left(-\frac{k_{\perp}^2}{2eB}, m+1, \frac{eBr^2}{2}\right) \quad (91)$$

The increasing hypergeometric function ${}_1F_1$ may overcome the pre-factor $e^{-\frac{eBr^2}{4}} r^m$, and become dominant at large r . However, for large degeneracies with $N \gg 1$ this does not take place. Indeed, in the parameter range discussed here with $N = 100$ and $M = -\sqrt{eB}$, the edge solution for $m = 0$ reads $k_{\perp}^2 \approx -10^{-42}eB$ and for k_{\perp} this small, the hypergeometric function remains almost constant for all r . This edge mode is simply the deeply confined LLL mode $e^{-\frac{eBr^2}{4}}$. For $m = 80$, the edge solution is about $k_{\perp}^2 \approx -0.4eB$. The ${}_1F_1$ function for this value at the edge is about 2 times the value at the origin or $r = 0$, which should be viewed as a moderate enhancement of the LLL wave function with ${}_1F_1$ set to 1. Specifically, $r^m e^{-\frac{eBr^2}{4}}$ for $m \approx N$ already peaks near the boundary, the edge enhancement by ${}_1F_1$ changes nothing qualitatively. For large N , the LLL wave function remains a good approximation for the low lying modes and needs no further amendment. The only effect is that the energy of these edge states become slightly lighter (for the case considered it is 0.8:1), which could turn to a moderate statistical enhancement.

X. NEGATIVE μ IN 1+2

The use of a negative potential μ maybe more than academic in 1+2 dimensions, since effective descriptions of planar condense matter systems are described by the model we presented in the main text using Dirac fermions [12]. In Fig. 10 we show the behavior of the effective potential \mathcal{V} as a function of σ for $T = 0$ and $\Omega = 0$, but large negative $\mu = -0.031\sqrt{eB}$, where the gap solution is lost (top). The critical value for which this happens is $\mu_c = -0.025\sqrt{eB}$. Amusingly, with increasing Ω , the mass gap is recovered at Ω_{c1} , then lost at Ω_{c2} . For instance, at $T = 0$ and $\mu = -0.03\sqrt{eB}$, we have $\Omega_{c1} = 0.00011\sqrt{eB}$ and $\Omega_{c2} = 0.00096\sqrt{eB}$ as illustrated in Fig. 10 middle and bottom respectively. In Fig. 11 we show the effective mass as a function of Ω for also $T = 0$ and $\mu = -0.03\sqrt{eB}$.

XI. FREE DIRAC FERMIONS IN 1+3

In 1+3 dimensions, the rotating metric (1) is minimally changed to $ds^2 \rightarrow ds^2 - dz^2$, with the pertinent changes to the co-moving coordinates. In the chiral Dirac basis for the gamma matrices, the rotating LL levels (6) are now changed to

The quantized fields are now

$$(E^\pm + \Omega(m - n + \frac{1}{2})) = \pm\sqrt{p^2 + M^2 + 2eBn} = \pm\tilde{E} \quad (92)$$

with the corresponding wavefunctions for particles

$$\begin{aligned} u_{nm1}^T &= e^{-iE^+t+ipz} \frac{1}{\sqrt{2\tilde{E}(\tilde{E}+p)}} \\ &\quad \times (Mf_{nm}, 0, (\tilde{E}+p)f_{nm}, -\sqrt{2eBn}f_{n-1,m}) \\ u_{nm2}^T &= e^{-iE^+t+ipz} \frac{1}{\sqrt{2\tilde{E}(\tilde{E}+p)}} \\ &\quad \times (\sqrt{2eBn}f_{nm}, (\tilde{E}+p)f_{n-1,m}, 0, Mf_{n-1,m}) \end{aligned} \quad (93)$$

and anti-particles

$$\begin{aligned} v_{nm1}^T &= e^{-iE^-t-ipz} \frac{1}{\sqrt{2\tilde{E}(\tilde{E}+p)}} \\ &\quad \times (Mf_{nm}, 0, -(\tilde{E}+p)f_{nm}, -\sqrt{2eBn}f_{n-1,m}) \\ v_{nm2}^T &= e^{-iE^-t-ipz} \frac{1}{\sqrt{2\tilde{E}(\tilde{E}+p)}} \\ &\quad \times (\sqrt{2eBn}f_{nm}, -(\tilde{E}+p)f_{n-1,m}, 0, Mf_{n-1,m}) \end{aligned} \quad (94)$$

$$\begin{aligned} \psi(t, \vec{x}) &= \int \sum_{mni} \frac{dp}{2\pi} \left(e^{-iE^+t+ipz} u_{nmi}(x_\perp) a_{nmi}(p) \right. \\ &\quad \left. + e^{-iE^-t-ipz} v_{nmi}(x_\perp) b_{nmi}^\dagger(p) \right) \end{aligned} \quad (95)$$

with the anti-commutation rules

$$[a_{nmi}(p), a_{pqj}(p')]_+ = \delta_{np}\delta_{mq}\delta_{ij}2\pi\delta(p-p') \quad (96)$$

-
- [1] A. Vilenkin, Phys. Rev. D **20**, 1807 (1979); A. Vilenkin, Phys. Rev. D **22**, 3080 (1980).
[2] S. Ebihara, K. Fukushima and T. Oka, Phys. Rev. B **93**, no. 15, 155107 (2016) [arXiv:1509.03673 [cond-mat.str-el]].
[3] D. E. Kharzeev, K. Landsteiner, A. Schmitt and H. U. Yee, Lect. Notes Phys. **871**, 1 (2013); [arXiv:1211.6245 [hep-ph]].
[4] Y. Liu and I. Zahed, arXiv:1509.00812 [hep-ph].
[5] K. Hattori and Y. Yin, Phys. Rev. Lett. **117**, no. 15, 152002 (2016) [arXiv:1607.01513 [hep-th]].
[6] Y. Jiang and J. Liao, Phys. Rev. Lett. **117**, no. 19, 192302 (2016) [arXiv:1606.03808 [hep-ph]].
[7] S. Ebihara, K. Fukushima and K. Mameda, Phys. Lett. B **764**, 94 (2017) [arXiv:1608.00336 [hep-ph]]; H. L. Chen, K. Fukushima, X. G. Huang and K. Mameda, Phys. Rev. D **93**, no. 10, 104052 (2016) [arXiv:1512.08974 [hep-ph]].
[8] G. E. Volovik, The Universe in a Helium Droplet (Oxford University Press, Oxford, 2003).
[9] M. N. Chernodub and S. Gongyo, JHEP **1701** (2017) 136 [arXiv:1611.02598 [hep-th]]; M. N. Chernodub and S. Gongyo, Phys. Rev. D **95**, no. 9, 096006 (2017) [arXiv:1702.08266 [hep-th]]; M. N. Chernodub and S. Gongyo, arXiv:1706.08448 [hep-th].
[10] R. Loganayagam, arXiv:1106.0277 [hep-th].
[11] V. P. Gusynin, V. A. Miransky and I. A. Shovkovy, Phys. Rev. D **52**, 4718 (1995) [hep-th/9407168].
[12] G. W. Semenoff and L. C. R. Wijewardhana, Phys. Rev. Lett. **63**, 2633 (1989).
[13] R. A. Janik, M. A. Nowak, G. Papp and I. Zahed, Phys. Rev. Lett. **81**, 264 (1998); [hep-ph/9803289]. M. A. Nowak, M. Sadzikowski and I. Zahed, Acta Phys. Polon. B **47**, 2173 (2016) [arXiv:1304.6020 [hep-ph]].
[14] I. A. Shushpanov and A. V. Smilga, Phys. Lett. B **402**, 351 (1997) [hep-ph/9703201].
[15] G. S. Bali, F. Bruckmann, G. Endrodi, Z. Fodor, S. D. Katz and A. Schafer, Phys. Rev. D **86** (2012) 071502 [arXiv:1206.4205 [hep-lat]].
[16] I. Zahed, Hydrodynamics of the Polyakov loop and Dirac spectra, 2015-11-04, SCGP video portal.
[17] F. Becattini, F. Piccinini and J. Rizzo, Phys. Rev. C **77**, 024906 (2008) [arXiv:0711.1253 [nucl-th]].
[18] Y. Jiang, Z. W. Lin and J. Liao, Phys. Rev. C **94**, no. 4, 044910 (2016) Erratum: [Phys. Rev. C **95**, no. 4, 049904 (2017)] [arXiv:1602.06580 [hep-ph]]; W. T. Deng and X. G. Huang, Phys. Rev. C **93**, no. 6, 064907 (2016) [arXiv:1603.06117 [nucl-th]].
[19] L. Adamczyk *et al.* [STAR Collaboration], Nature **548**, 62 (2017) [arXiv:1701.06657 [nucl-ex]].
[20] H. L. Chen, K. Fukushima, X. G. Huang and K. Mameda,

Phys. Rev. D **96**, no. 5, 054032 (2017) [arXiv:1707.09130 [hep-ph]].